Lasing on the self-photopumped nickel-like $4f\,^1P_1 \rightarrow 4d\,^1P_1$ x-ray transition

Joseph Nilsen, James Dunn, and Albert L. Osterheld
Lawrence Livermore National Laboratory, Livermore, California 94550

Yuelin Li
Institute for Laser Science and Applications, Lawrence Livermore National Laboratory, Livermore, California 94550

(Received 10 June 1999)

We demonstrate lasing on the nickel-like $3d^9\,4f\,^1P_1 \rightarrow 3d^9\,4d\,^1P_1$ x-ray laser line in Zr ($Z=40$), Nb ($Z=41$), and Mo ($Z=42$) and present measured wavelengths for these ions as well as predicted values for ions from $Z=36$ to 54. Lasing on this line was first predicted two years ago and has now been achieved. Unlike the usual collisional excitation laser, this line lases because radiation trapping allows a large radiation field to build up on the $3d^{10}\,^1S_0 \rightarrow 3d^9\,4f\,^1P_1$ resonance line and populate the $4f$ upper laser state by the self-photopumping process. For Ni-like Mo a gain of 13 cm^{-1} is measured on this transition at 226 Å for targets up to 1 cm long. [S1050-2947(99)51010-X]

PACS number(s): 42.55.Vc, 42.60.Lh, 32.30.Rj

Since the introduction of the prepulse or multiple pulse technique [1–3] most researchers now use some variant of these techniques to achieve lasing on the Ne-like $3p\,^1S_0 \rightarrow 3s\,^1P_1$ and Ni-like $4d\,^1S_0 \rightarrow 4p\,^1P_1$ laser lines. These techniques illuminate solid targets with several pulses, with the first pulse used to create a larger, more uniform preplasma that is at the right densities for gain and laser propagation and allows the subsequent pulses to be absorbed more efficiently and heat the plasma to lasing conditions. Most of those experiments were done with large kilojoule-size laser facilities designed for fusion research. Recently, tremendous progress has been made toward tabletop x-ray lasers by using a nanosecond prepulse followed by a picosecond drive pulse. Using less than 10 J of energy, lasing was demonstrated at 326 Å in Ne-like Ti [4] at the Max Born Institute (MBI) and at 146 Å in Ni-like Pd [5] at Lawrence Livermore National Laboratory (LLNL) using the COMET laser.

The Ne-like $3p\,^1S_0 \rightarrow 3s\,^1P_1$ and Ni-like $4d\,^1S_0 \rightarrow 4p\,^1P_1$ lines lase by having monopole collisional excitation from the ground state populate the upper laser level. The lower laser level is depopulated by fast radiative decay to the ground state. Unlike the usual collisional excitation laser, the $4f\,^1P_1 \rightarrow 4d\,^1P_1$ line lases because radiation trapping allows a large radiation field to build up on the $3d\,^1S_0 \rightarrow 4f\,^1P_1$ resonance line and populate the $4f$ upper laser state by the self-photopumping process. For convenience we leave out the $3d^9$ electrons that are common to both states.

In this paper we demonstrate lasing on the Ni-like $4f\,^1P_1 \rightarrow 4d\,^1P_1$ x-ray laser line in Zr, Nb, and Mo using the COMET laser at LLNL and present measured wavelengths for these ions as well as predicted values for other nearby ions. This is a new class of self-photopumped Ni-like x-ray laser, which was first predicted two years ago [6]. For Ni-like Mo a gain of 13 cm^{-1} is measured on this transition at 226 Å for targets up to 1 cm long. We compare our measured wavelengths with calculated wavelengths [7] based on experimentally determined energies for the upper and lower levels for Zr, Nb, and Mo. Using the experimental data to provide small corrections to our theoretical calculations, we predict the wavelength of this transition for ions from $Z=36$ to 54.

To understand the laser mechanism for the Ni-like Mo $4f\,^1P_1 \rightarrow 4d\,^1P_1$ laser line at 226 Å, Fig. 1 shows the energy-level diagram, including typical transition rates in $nsec^{-1}$ for the important levels involved. The $4f\,^1P_1$ upper laser level is populated by a combination of collisional excitation and radiative excitation (self-photopumping) of the Ni-like ground state. The $3d\,^1S_0 \rightarrow 4f\,^1P_1$ resonance line is optically thick so that radiative trapping on this transition allows a large radiation field to build up. Under typical lasing conditions described below, the radiation field becomes large

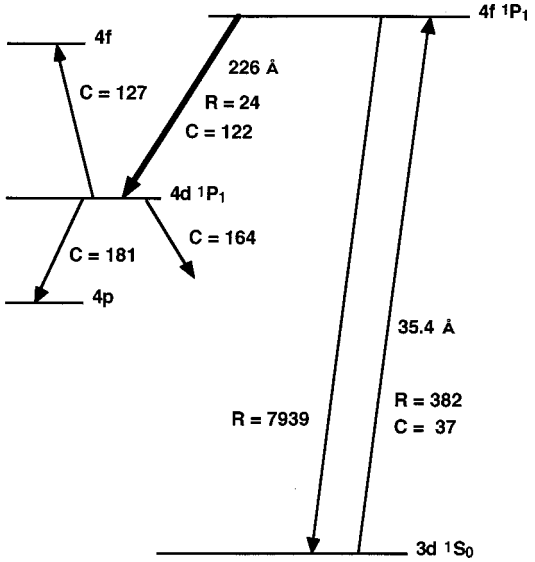

FIG. 1. Energy-level diagram showing the laser mechanism for the Ni-like Mo $4f\,^1P_1 \rightarrow 4d\,^1P_1$ x-ray laser line. The collisional (C) and radiative (R) rates are given per nanosecond for typical plasma conditions with electron density of $6.3\times10^{19}\,cm^{-3}$, electron temperature of 295 eV, and an ion temperature of 47 eV. Lasing is driven by the strong photopumping from the $3d\,^1S_0$ ground state populating the $4f\,^1P_1$ upper laser level.

enough that the photopumping rate is an order of magnitude larger than the collisional excitation rate and becomes the primary mechanism that populates the upper laser level. The $4f\,^1P_1$ level lases to the $4d\,^1P_1$ lower laser state. The lower laser state is depopulated primarily by collisional transfer to other nearby $4f$ and $4p$ levels.

To model the x-ray laser experiments we use the LASNEX code [8] to calculate the heating and hydrodynamics of the x-ray laser target by the optical drive laser. The temperatures, densities, and velocities calculated by LASNEX are then used as input to the XRASER code [9], which calculates the detailed kinetics and gain, including the effects of radiation transport on the strong $3d\rightarrow 4p$ and $4f$ resonance lines. For this modeling we used a 1-J, 600-psec full width at half maximum (FWHM) Gaussian prepulse to illuminate the target followed 700 psec later by a 5-J, 1-psec FWHM Gaussian pulse. The delay between the pulses is peak to peak. The energy was deposited in a 1.2-cm-long by 120-μm-wide line. The LASNEX calculations were done in one dimension (1D) but did include an expansion angle of 15° in the dimension perpendicular to the primary expansion so as to simulate 2D effects.

In the calculations, the gain of the 226-Å laser line peaks about 1 psec after the peak of the short pulse at 27 μm from the target surface with a peak gain of 160 cm^{-1}. The very high gain falls by half within 2 psec, but gain greater than 20 cm^{-1} does persist for 8 psec after the short pulse. In Fig. 1 we show rates typical for the plasma at 5 psec after the peak of the short pulse at 50 μm from the target surface. The optical depth of the $3d\,^1S_0\rightarrow 4f\,^1P_1$ resonance line is 100 and the line strength is 0.0163 photons per mode. The gain is 37 cm^{-1} with an electron temperature of 295 eV, an ion temperature of 47 eV, an ion density of $4.42\times 10^{18}\,\mathrm{cm}^{-3}$, and an electron density of $6.30\times 10^{19}\,\mathrm{cm}^{-3}$. The gain profile has a spatial FWHM width of 60 μm. The gradient in the electron density is $-1.69\times 10^{22}\,\mathrm{cm}^{-4}$. For a 226-Å x ray, this gradient would refract the x ray by only 19 μm over a 1-cm propagation length. The collision rates shown for the lower laser state are net rates out of the level. In the absence of photopumping the gain disappears and goes slightly negative.

In Ne-like ions lasing has been observed on an analogous self-photopumped $3d\,^1P_1\rightarrow 3p\,^1P_1$ laser line in S [10], Ar [11], and Ti [12]. Several references [13,14] discuss this lasing mechanism in detail. It is interesting to note that the intensity of the self-photopumped Ne-like Ti $3d\,^1P_1\rightarrow 3p\,^1P_1$ laser line can dominate the output of the usual Ne-like Ti $3p\,^1S_0\rightarrow 3s\,^1P_1$ in sufficiently long plasmas [12]. This suggests that the Ni-like $4f\,^1P_1\rightarrow 4d\,^1P_1$ laser line could become the dominant line under suitable plasma conditions.

The laser experiments were performed on the COMET Laser Facility at Lawrence Livermore National Laboratory. To make these materials lase, we use a 1-J, 600-psec FWHM pulse to preform and ionize the plasma followed by a 5-J, 1-psec pulse to heat the plasma. The delay between the two pulses is 700 psec. The beams are focused to a 70-μm×1.25-cm line onto the slab targets that vary in length up to 1 cm. The long pulse is defocused a factor of 2 to ensure better overlap between the beams from the long and short pulse. A five-segmented stepped mirror is used to provide traveling-wave illumination of the target at the speed of light. The main diagnostics is an on-axis flat-field grating spectrometer coupled to a thinned-backside-illuminated charge-coupled device (CCD) camera. Each CCD pixel corresponds to approximately 0.17 to 0.20 Å across the range of the spectrometer from 140 to 330 Å.

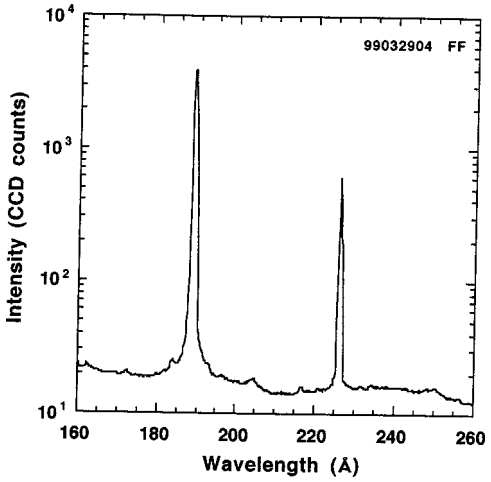

FIG. 2. On-axis spectrum of a 0.9-cm-long Mo target showing two lasing lines: the $4d\,^1S_0\rightarrow 4p\,^1P_1$ lasing line at 189 Å and the $4f\,^1P_1\rightarrow 4d\,^1P_1$ laser line at 226 Å. The 189-Å line is saturated on the CCD.

Figure 2 shows an on-axis Mo spectrum with the strong $4d\,^1S_0\rightarrow 4p\,^1P_1$ line lasing at 189 Å and the weaker $4f\,^1P_1\rightarrow 4d\,^1P_1$ line lasing at 226 Å. The 189-Å line is saturated on the detector so the ratio between the lines is larger than depicted. However, the 226-Å line is lasing very well and both lines completely dominate the background emission. Lasing on the $4d\,^1S_0\rightarrow 4p\,^1P_1$ line in Ni-like Mo and other nearby ions has been discussed in two recent papers [15,16] and will not be discussed further here.

To understand how well the 226-Å line was lasing we did a gain length study by using 0.1-cm-thick polished Mo targets that varied in length from 0.2 to 0.9 cm. In Fig. 3 we

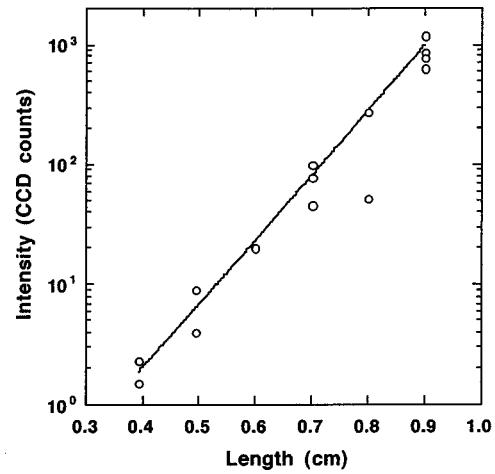

FIG. 3. Intensity versus length for the Ni-like Mo $4f\,^1P_1\rightarrow 4d\,^1P_1$ x-ray laser line. The experimental data are shown by circles, while the fit to the Linford formula is given by the solid line. The fitted gain is 13 cm^{-1}.

TABLE I. Wavelengths (in angstroms) of the $3d^9\,4f\,^1P_1 \rightarrow 3d^9\,4d\,^1P_1$ transition in Ni-like ions as measured in x-ray laser experiments, as calculated from the difference of experimentally determined energies [7], and as predicted by the MCDF code after small experimentally based corrections. The uncertainty in the last digit is given in parentheses.

Z	Laser measurement	Calculated from experimental energies	Predicted wavelengths
36 (Kr)			443.4
37 (Rb)		383.9(2)	383.6
38 (Sr)		337.1(2)	337.3
39 (Y)		300.4(2)	300.6
40 (Zr)	271.0(2)	270.8(3)	270.9
41 (Nb)	246.4(3)	247.0(5)	246.5
42 (Mo)	226.0(3)	226.7(5)	226.1
43 (Tc)			208.9
44 (Ru)			194.1
45 (Rh)			181.3
46 (Pd)			170.1
47 (Ag)			160.4
48 (Cd)			151.8
49 (In)			144.7
50 (Sn)			135.5
51 (Sb)			129.6
52 (Te)			124.0
53 (I)			118.8
54 (Xe)			114.0

show the intensity versus target length for the $4f\,^1P_1 \rightarrow 4d\,^1P_1$ lasing line at 226 Å. Using the Linford formula [17], we estimate a gain of 13 cm^{-1}. There is no sign of saturation in this figure. In our modeling we estimate the saturation intensity of the 226-Å line at 9 $GW\,cm^{-2}$ under the plasma conditions at the time of peak gain. This is almost three times the saturation intensity estimated for the 189-Å line and indicates that while the 226-Å line is weaker and has lower gain it does have the potential to be the stronger line.

We have also observed lasing on the $4f\,^1P_1 \rightarrow 4d\,^1P_1$ line in Ni-like Zr and Nb. We have not done a detailed gain length study of these ions with the traveling-wave setup, but have done some earlier experiments without the traveling wave in which we measured weak gain. For Ne-like ions the hyperfine effect was observed to cause even Z ions to lase much better than odd Z ions [18]. For these Ni-like ions we estimate that the hyperfine effect reduces the gain by less than 1% for the odd Z ions such as Nb, and therefore we expect that Zr and Nb will produce output similar to Mo when optimized with the traveling-wave setup. The use of the traveling-wave setup does increase the output of the $4f\,^1P_1 \rightarrow 4d\,^1P_1$ laser line in Mo by two orders of magnitude and is essential for observing strong lasing on this line. The wavelengths of the measured laser lines with their uncertainties are given in Table I. The error bar given is determined by the accuracy of determining the peak of both the reference lines and the measured lines and is between 0.2 and 0.3 Å. Reference [16] has more detail about the calibration of the spectrometer.

The $4f\,^1P_1 \rightarrow 4d\,^1P_1$ line has not been observed directly in nonlasing plasmas, but its wavelength can be calculated by using the measured values of the $3d\,^1S_0 \rightarrow 4f\,^1P_1$ resonance line [19] together with the experimentally determined values for the energy of the $4d\,^1P_1$ lower laser state [20]. This approach is described in Ref. [7] and the experimentally based wavelengths for $Z=37$ to 42 are given in Table I along with their uncertainties. For $Z=40$ to 42 these values agree with the values measured in the x-ray laser experiments within the experimental uncertainties. The maximum disagreement is 0.7 Å.

We calculated the wavelengths of the laser lines using the multiconfiguration Dirac-Fock (MCDF) atomic physics code of Grant *et al.* [21] in the extended average level (EAL) mode. EAL calculations were done separately for the $J=1$ even and odd parity states. The energies of the $4f\,^1P_1$ and $4d\,^1P_1$ level were subtracted to calculate the energy of the laser transition. The upper laser level is always dominated by the $4f\,^1P_1$ configuration and is easy to identify by its configuration. However, the lower laser level has substantial mixing between the *LS* configurations. For example, in Ni-like Mo, the lower laser state is a mixture of $0.661\,4d\,^1P_1 - 0.622\,4d\,^3P_1 - 0.328\,4d\,^3S_1$. This level can be more easily identified by ordering the energies of all the $J=1$ even parity states. It is level number 4 starting from the lowest energy.

We then fit the difference between the energies calculated by the MCDF code and the experimentally determined energies for $Z=37$ to 42 to a straight line. For $Z=40$ to 42 we weigh the two experimentally based values by their uncertainties. We then adjust the MCDF calculation by subtracting this fitted curve, which has a value of $-4.011+0.11385*Z$ in eV. For $Z=42$ this amounts to a 0.77-eV correction. The wavelengths predicted by this method are given in Table I for $Z=36$ to 54. We believe these values are accurate to better than 1 Å.

In this work, we demonstrate lasing on the Ni-like $4f\,^1P_1 \rightarrow 4d\,^1P_1$ x-ray laser line in Zr, Nb, and Mo as was first predicted two years ago. The measured wavelengths for these ions are presented. In contrast to the usual collisional excitation laser, this line lases because radiation trapping allows a large radiation field to build up on the $3d\,^1S_0 \rightarrow 4f\,^1P_1$ resonance line and populate the $4f$ upper laser state by the self-photopumping process. For Ni-like Mo a gain of 13 cm^{-1} is measured on this transition at 226 Å for targets up to 1 cm long. We predict the wavelength of this transition for ions from $Z=36$ to 54 using the experimental data to provide small corrections to our theoretical calculations. These experiments show how this new self-photopumping mechanism can produce strong lasing on the Ni-like $4f\,^1P_1 \rightarrow 4d\,^1P_1$ x-ray laser line and suggests that this line could dominate the laser output under the right plasma conditions.

This work was performed under the auspices of the U.S. Department of Energy by the Lawrence Livermore National Laboratory under Contract No. W-7405-ENG-48. The authors would like to thank A. N. Ryabtsev and S. S. Churilov for their valuable advice and Jim Hunter, Hedley Louis, and Tony Demiris for technical support for the experiments.

[1] J. Nilsen, B. J. MacGowan, L. B. Da Silva, and J. C. Moreno, Phys. Rev. A **48**, 4682 (1993).
[2] J. C. Moreno, J. Nilsen, and L. B. Da Silva, Opt. Commun. **110**, 585 (1994).
[3] J. Nilsen and J. C. Moreno, Phys. Rev. Lett. **74**, 3376 (1995).
[4] P. V. Nickles, V. N. Shlyaptsev, M. Kalachnikov, M. Schnuerer, I. Will, and W. Sandner, Phys. Rev. Lett. **78**, 2748 (1997).
[5] J. Dunn, A. L. Osterheld, R. Shepherd, W. E. White, V. N. Shlyaptsev, and R. E. Stewart, Phys. Rev. Lett. **80**, 2825 (1998).
[6] J. Nilsen, J. Opt. Soc. Am. B **14**, 1511 (1997).
[7] A. N. Ryabtsev, S. S. Churilov, J. Nilsen, Y. L. Li, J. Dunn, and A. L. Osterheld, Opt. Spectrosc. (to be published).
[8] G. B. Zimmerman and W. L. Kruer, Comments Plasma Phys. Control. Fusion **2**, 51 (1975).
[9] J. Nilsen, in *Atomic Processes in Plasmas*, edited by Allan Hauer and A. L. Merts, AIP Conf. Proc. No. 168 (AIP, Woodbury, NY, 1998), pp. 51–58.
[10] Y. L. Li, P. X. Lu, G. Pretzler, and E. E. Fill, Opt. Commun. **133**, 196 (1997).
[11] J. Nilsen, H. Fiedorowicz, A. Bartnik, Y. L. Li, P. X. Lu, and E. E. Fill, Opt. Lett. **21**, 408 (1996).
[12] M. P. Kalachnikov, P. V. Nickles, M. Schnürer, W. Sandner, V. N. Shlyaptsev, C. Danson, D. Neely, E. Wolfrum, J. Zhang, A. Behjat, A. Demir, G. J. Tallents, P. J. Warwick, and C. L. S. Lewis, Phys. Rev. A **57**, 4778 (1998).
[13] J. Nilsen, Phys. Rev. A **53**, 4539 (1996).
[14] J. Nilsen, Phys. Rev. A **55**, 3271 (1997).
[15] J. Dunn, J. Nilsen, A. L. Osterheld, Y. L. Li, and V. N. Shlyaptsev, Opt. Lett. **24**, 101 (1999).
[16] Y. L. Li, J. Nilsen, J. Dunn, A. L. Osterheld, A. Ryabtsev, and S. Churilov, Phys. Rev. A **58**, R2268 (1998).
[17] G. J. Linford, E. R. Peressini, W. R. Sooy, and M. L. Spaeth, Appl. Opt. **13**, 379 (1974).
[18] J. Nilsen, J. A. Koch, J. H. Scofield, B. J. MacGowan, J. C. Moreno, and L. B. Da Silva, Phys. Rev. Lett. **70**, 3713 (1993).
[19] N. Schweitzer, K. Klapisch, J. L. Schwob, M. Finkenthal, A. Bar-Shalom, P. Mandelbaum, and B. S. Fraenkel, J. Opt. Soc. Am. **71**, 219 (1981).
[20] A. N. Ryabtsev, S. S. Churilov, and J. F. Wyart, Opt. Spectrosc. **62**, 153 (1987).
[21] I. P. Grant, B. J. McKenzie, P. H. Norrington, D. F. Mayers, and N. C. Pyper, Comput. Phys. Commun. **21**, 207 (1980).